Estimating precipitation from radar observations in the trade-wind cumulus region

Louise Nuijens

October 9, 2005

WAGENINGEN UR
For quality of life

Estimating precipitation from radar observations in the trade-wind cumulus region

MSc Thesis - Louise Nuijens

October 9, 2005

Wageningen University and Research Center, Meteorology and Air Quality Section,
Building no.403, Duivendaal 2, 6701 AP Wageningen, The Netherlands.
E-mail: louise.nuyens@wur.nl

Thesis advisors:

Prof.Dr.B.Stevens
University of California, Los Angeles

Dr.J.Vilà-Guerau de Arellano
Wageningen University and Research Center

Cover photographs (from left to right, top to bottom):
1. Shallow precipitating cloud
2. Shallow cumulus field located above Barbuda
3. Shallow cumulus cloud near the coast of Barbuda
4. The S-PolKa radar

Photographs 1, 2 and 4 are courtesy of B.Stevens

Abstract

In past years the role of shallow cumulus clouds has been primarily the one of effective evaporators. Recently, the precipitation associated with shallow clouds and the possibly significant influence of this on a larger scale environment is receiving more attention. One of the main purposes of the Rain In Cumulus over the Ocean (RICO) field study was to study precipitation from shallow clouds. RICO was conducted in a region in the vicinity of the Caribbean islands Antigua and Barbuda during a 66-day period associated with a persistent trade-wind regime. High-resolution data collected during RICO by the S-PolKa radar, located on Barbuda, has provided detailed information of clouds and precipitation in an area with a radius of 150 km. By exploring this extensive dataset, this study aims at giving a first indication of the frequency and total amount of rainfall that occurs in the trade-wind region.

To achieve this, horizontal radar scans are processed that allow to study rainfall at heights below cloud top even at large distances from the radar. Time series of area rainfall reveal that shallow precipitation is prevalent during RICO and that at least 50% of the total rain is associated with precipitation from shallow clouds. A couple of days characterized by heavier rain can be related to periods of deeper convection under unstable conditions. The overall average area rain rate and echo coverage were 0.72 mm day^{-1} and 1.72% respectively. These first estimates may indicate that precipitation from shallow clouds is certainly not negligible and may have a significant influence on cloud and boundary layer development. The relative rainfall amounts derived from S-PolKa coincide well with raingauge measurements on the surface station on Barbuda, suggesting shallow precipitation often reaches the surface. The structure and organization of rain echoes, as observed from the extensive collection of radar scans, is very diverse. This raises many interesting questions regarding the relation between various cloud types and the precipitation they produce. This dataset is a great opportunity to explore these issues into more detail in future research.

Contents

Chapter 1

Introduction

Shallow cumulus clouds prevail over much of the world's oceans and land. They are ubiquitous over the oceans in the trade-wind regions located between 30°N and 30°S, outside of the Intertropical Convergence Zone (ITCZ). These trade-wind regions, named after the former trade routes, are marked by persistent eastward and equator ward winds, resulting in northeasterlies and southeasterlies in the northern and southern hemisphere respectively. The boundary layer in the trade-wind region is capped by the trade inversion, *i.e.* a zone of increasing temperature with height, dividing the moist cool easterlies in the well-mixed layer from the dry westerlies in the free atmosphere. Towards the equator, as the oceans become warmer and the tropospheric stability lower, the inversion height increases.

The easterly trade-winds meet at the ITCZ and fuel deep convection that is common in those regions. The trade-winds thereby play an important role in the global Hadley circulation, illustrated in Figure 1.1. At high altitudes in the ITCZ the flow diverges north- and southwards again, and the Hadley circulation is completed with a subsidence region over the colder oceans toward the subtropics. These latitudes, especially near eastern boundary currents, are marked by a lower trade inversion and a persistent stratocumulus-topped boundary layer.

The trade-winds transport relatively dry air and induce the evaporation from the oceans surface. Driven by latent heat fluxes and buoyancy, cumulus clouds grow into the boundary layer and deepen it, by mixing dry air downwards and moist air upwards. During suppressed wintertime conditions, hindered by the trade inversion, the clouds are shallow (1-2 km) with a cloud top mostly confined below the freezing level, typically near 5 km (LeMone and Pennell 1976; Neggers 2002; Stevens 2005).

Shallow cumulus clouds occur in a wide variety of shapes, for example as organized cloud lines, as patches (clusters) with emerging tops or as active deeper cumulus congestus. Some examples of shallow cumulus are shown on the cover photographs.

The ability of shallow cumulus to enhance (latent) heat fluxes, to mix air inside the boundary layer and deepen it by evaporation at the top, has given them the status of effective evaporators. By doing so they may serve as fuel, in the form of moisture, for the deep convection in the ITCZ. Despite their low cloud fraction, of about 15-20% (Siebesma et al. 2003), the wide-spread coverage of shallow cumulus makes them crucial for the global Hadley-circulation and climate feedback processes, through their influence on both the hydrological cycle and the incoming shortwave radiation.

Recent research projects that focused on the tropical western Pacific warm pool, the

region on earth with the highest annual rainfall, indicate the existence of shallow cumulus in 'trade-like regimes', when the atmosphere is more suppressed. These regimes are prominent enough to impact the seasonal distributions of heating and moistening of the boundary layer and to prepare the atmosphere for deeper convection (Johnson and Lin 1997; Rickenbach and Rutledge 1998; Johnson et al. 2001). It is even suggested that shallow and deep convection must coexist to maintain a neutrally stable atmosphere (Wu 2003).

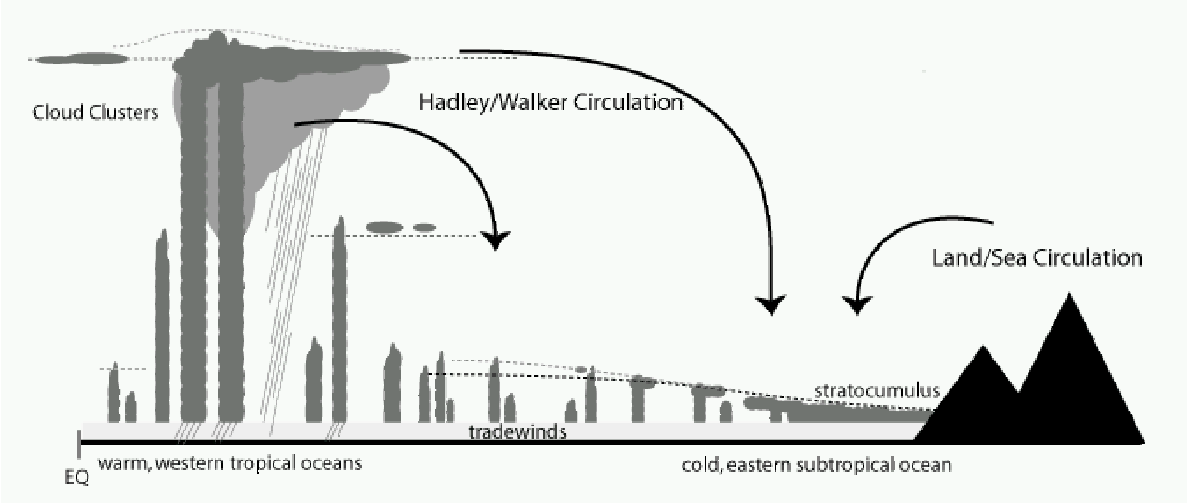

Figure 1.1: The three cloud regimes in the global Hadley circulation, driven by temperature differences of subtropical and tropical oceans. From: Stevens (2005).

In previous years, the role of shallow cumulus is believed to have been primarily the one of evaporator. Although precipitation from shallow clouds, *i.e.* shallow precipitation, has been observed, actual quantitative estimates have been lacking. Until now, precipitation processes were assumed negligible when modeling shallow cumulus, for example with Large Eddy Simulation (LES). Recently, observational studies have given the first quantitative estimates of shallow precipitation over the tropical oceans. Petty (1999) combined surface synoptic reports with satellite infrared images and concluded that shallow clouds were associated with 20-40% of the non-drizzle precipitation observations over much of the ocean east of Australia. Short and Nakamura (2000) used data derived from a spaceborn precipitation radar and estimated that shallow precipitation accounts for 22% of the total rainfall over tropical oceans during both winter and summer seasons.

Shallow precipitation may also have a significant impact on cloud processes on many scales. It is likely that precipitation not only affects the microphysical properties of a cloud (on the microscale), but also the organization and interaction among clouds (on the mesoscale). An example of the influence of precipitation on the mesoscale is the occurrence of so-called 'cold pools'. Cold pools are the regions of cold and moist air below mature cumulus clouds, created by the evaporation of drizzle. During the recovery of cold pools, their moisture content and temperature increase rapidly by enhanced sea surface fluxes, so that a region of air is created where only a small vertical lifting is needed to trigger new convection (Jensen et al. 2000; Tompkins 2001).

On a larger scale, the extensive coverage of shallow cumulus fields can have a consid-

erable impact on the radiation budget and climate of the earth. Also, the shallow heating from these clouds, *i.e.* heating associated with moist convection below the inversion layer, can be an important component of heat and enery budgets over the tropical oceans, although this remains something of an open question (Johnson and Lin 1997; Lau and Wu 2003; Wu 2003).

The statistics of precipitating cloud fields and the variety of shapes in which they occur has been the focus of studies of other moist convection regimes such as stratocumulus and deep convective clouds. However, no such objective has been applied to shallow cumulus in past research, until now. In December 2004 and January 2005, the Rain in Cumulus over the Ocean (RICO) field study was conducted with the purpose of observing and understanding shallow cumulus at all relevant scales, with specific attention to the role of precipitation processes. RICO took place in the vicinity of two small islands in the Caribbean, Antigua and Barbuda: a region associated with a persistent trade-wind regime during the winter months. In the operational phase of RICO, a ground-based radar (the NCAR S-PolKa radar), located on Barbuda, made observations of clouds and precipitation with a high resolution covering an area with a radius of ~ 150 km.

The objective of this study is to follow up on previous research and obtain estimates of precipitation, but specifically for the trade-wind region during RICO and for a time period of slightly more than two months. This is accomplished by exploring the extensive dataset gathered by the S-PolKa radar. This dataset offers unique opportunities to study rainfall statistics on a larger scale and with a higher resolution, in both space and time, than has been done in previous studies. The following questions are addressed:

- With what frequency and intensity does precipitation occur, if at all?
- What are typical rain rates produced by shallow cumulus?
- Does the precipitation change significantly over the RICO period, for different cloud types, or for different areas?
- How do the radar derived rain rates compare to rainfall estimates from other instruments, such as surface rain gauge measurements or those inferred from satellite measurements?

By giving a first impression of the precipitation, the answers to these questions may provide a basis upon which subsequent case studies can be selected. Furthermore, if the radar data set is proven to be successful and effective for the purpose of mapping precipitation on a larger scale, the study can be extended towards providing datasets of rainfall statistics for LES and other models.

This report proceeds as follows: in Chapter 2 a more detailed description is given on the scientific goals and implementation of the RICO experiment in the trade-wind region. An explanation of the radar data and our analysis procedures are described in Chapter 3. Results and answers to the above questions are discussed in Chapter 4. Lastly, conclusions are given in Chapter 5 with recommendations for future research on precipitation in shallow cumulus.

Chapter 2

The RICO field study

2.1 Scientific goals

Studies in the past have focused mainly on understanding the dynamics and microphysical processes in shallow cumulus on a (single) cloud scale. Precipitation in shallow cumulus involves many processes on a microscale, but it can also be of major importance to the mesoscale organization of clouds. On an even larger scale it may have a significant impact on the heat, moisture and energy budgets in the tropics, and hence our climate. The RICO field study was special, because research efforts at all relevant scales were combined resulting in a collaboration of researchers with many different scientific objectives. RICO is an initiative of researchers from American universities, the National Center of Atmospheric Research (NCAR) in the United States and many other international universities and research centers. The overall scientific goal of RICO is to understand and describe the characteristics of the trade-wind cumuli and all the processes involved, with special attention to precipitation processes. Consequently the different objectives can be divided into 1) the micro scale (micrometers to a kilometer), 2) meso scale (one kilometer to tens of kilometers) and 3) the large scale (tens of kilometers and larger) with the following general scientific questions:

1. How can the fast onset of precipitation in shallow cumulus clouds be explained?
2. What is the influence of convective processes, precipitation in specific, on the organization and structure of shallow cumulus cloud fields?
3. What are the statistics of a (precipitating) shallow cumulus cloud field and is its effect on energy budgets and climate significant? (Rauber et al. 2004)

2.2 Location and instrumentation

The RICO field study took place from the 21$^{\text{st}}$ of November (2004) to the 25$^{\text{th}}$ of January (2005) in the region around the Caribbean islands of Antigua and Barbuda, see Figure 2.1(a), where trade-wind cumulus clouds frequently occur. On a satellite image of November 22$^{\text{nd}}$, 2004 for example shown in Figure 2.1(b), several extended fields of cumulus north of Barbuda are visible. The fields of smaller cumulus clouds southeast of Antigua are harder to distinguish. Radar images of earlier studies have shown that precipitation is

prevalent in this area during the winter months. This period was also chosen to avoid hurricanes, fronts and periods of deep convection. Most of the measurements were conducted upwind of the islands, in an area fully exposed to the undisturbed trade-winds.

(a) Figure a. The Caribbean with Antigua & Barbuda in rectangle box

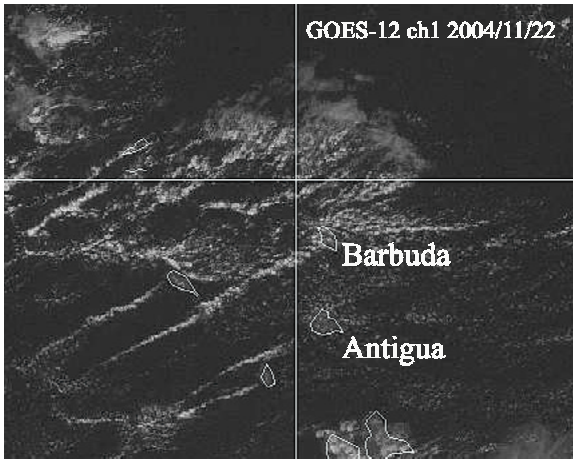

(b) Figure b. GOES satellite image of Nov 22, 2004

Figure 2.1: Location of the RICO field study

In November of 2004 only the (NCAR) S-PolKa radar, a very effective instrument for observing clouds and precipitation, operated from its location on the island of Barbuda. With S-PolKa the development and lifetime of cumulus clouds in a large area was studied in more detail to determine flight and radar strategies for the following period. During the second period in December 2004 and January 2005, an extensive dataset was collected by three research aircrafts (NCAR-C130, University of Wyoming King Air, the United Kingdom BAE-146), one research vessel (RV Seward Johnson), a surface station on Barbuda, sounding operations and several ground-based aerosol measuring sites on Antigua and Puerto Rico. Research flights were coordinated with the radar and the aircrafts performed short intercomparison flights on a couple of occasions. A wide variety of instruments was carried on board of all aircrafts and the ship, including a dropsonde system, lidars, several (Doppler) cloud radars and instruments to measure basic atmospheric variables, basic cloud microphysics, trace gas chemistry, and detailed cloud and aerosol properties. Real time satellite information completed this dataset. All of these data are collected in a RICO Data Archive Center (RDAC), which will be available for public use in February of 2006.

2.3 The weather conditions

As compared to climatological data from Antigua, the weather conditions during December 2004 and January 2005 in the trade-wind region were not far from normal. The domain was dominated by shallow cumulus clouds in the form of bands, clusters and scattered cells. Winds were on average easterly with a speed of about 11 kts. Rainfall amounts recorded on the V.C.Bird International Airport at Antigua were somewhat below the climatological

average.

The weather was influenced by the expected phenomena during this time period, such as a few tropical waves, low level troughs, some upper level troughs and a few weak cold fronts at the end of the field phase. Less than 5% of the period was overcast or dominated by very deep convective conditions and rainfall was usually a result of convection induced by the trade winds and to a lesser extent by lifting cold fronts (shear lines). On some days, the clouds over the Atlantic Ocean were very shallow and sparse. At the start and end of the field phase, the depth of the easterly trade-winds was very low and the upper level westerlies strengthened and were even observed as low as 700 mb. It was noted that the depth of the easterlies, sometimes extending even above the freezing level, was closely related to the observation of showers.

In general, the weather reports indicate that the weather during RICO allowed for good observational conditions to study trade-wind cumulus and its precipitation (Caesar 2005).

2.4 Research and education: the student research flight

A very unique part of the RICO study was the combination of research and education, by offering the RICO Graduate Seminar Series (RGSS) and a research flight designed and directed by students. The RGSS consisted of seminars presented by the researchers involved in the field and excursions on board the ship and the aircrafts. The goal of the student research flight was to allow students to participate in the process of identifying scientific objectives and developing a flight plan. This required a good collaboration between all students at all the phases during the project. 17 MSc and PhD students from the US and Europe were involved in this research flight. Two different plans were presented to the RICO principal investigators and both were approved. One of the main objectives was to study and understand the processes that control the formation of the 'island tails', a line of clouds that frequently form off the leeward coast of the Caribbean islands, extending several kilometers downwind. These tails can be observed in Figure 2.1(b). One of the mysteries of the island tails when observing satellite images is the fact they sometimes seem to develop at places in the open ocean where no island is present, perhaps indicating the presence of rocks. Also, the smallest islands usually have the longest tails. The most important scientific questions to be addressed are:

1. Are the clouds forced by an island heating effect or other dynamic processes?
2. Do the islands serve as a source for aerosol particles that may act as nucleation sites?
3. Where in the tails does precipitation occur, if at all, and how may this influence the lifetime of the tail clouds?

The island tail objective was implemented successfully during a research flight with the NCAR C-130 on January the 18^{th} when measurements were made in an island tail off the coast of Barbuda. All students participated in this flight by taking in relevant positions within the aircraft, the operations center and at the radar site. Students were and will be encouraged to take the opportunity to analyze this dataset and to present papers with new results and insights in the processes controlling these island tails.

Chapter 3

Data processing

3.1 The S-PolKa radar data

The National Center of Atmospheric Research (NCAR) S-band Polarization (S-Pol) radar, located on Barbuda (17.6°36.448' N, 61°49.457' W), collected data during the full operational period of RICO. The ground-based S-Pol radar with a parabolic shaped antenna and a 10.68 cm wavelength (S-band) is an effective instrument in measuring precipitation from clouds. The radar was also equipped with a second wavelength of 8.6 mm (K-Band) and is therefore sometimes referred to as the SPolKa radar. Besides its high resolution on the scale of convective processes, this radar has an extensive coverage of up to 150 km in diameter. This makes it possible to map precipitation on a mesoscale and to create an attractive dataset for the purpose of this study. Among the many variables measured by S-Pol, the *radial velocity* and *radar reflectivity* are the most essential for this data analysis.

The *radial velocity* V_R ($\mathrm{m\,s^{-1}}$) is estimated by comparing the frequency of the returned radar signal with the transmitted signal, using the Doppler frequency shift theory. It is therefore a measure of the motions in the radar volume along the radar line of sight. Targets moving toward the radar have a negative velocity, while targets moving away from the radar have a positive velocity. For nearly horizontal scans it can be assumed that the motion of targets along the radar beam is due only to the ambient wind, thus allowing the horizontal wind field (speed and direction) to be estimated. For a more detailed explanation of the radial velocity see Appendix A.

The returned power of the transmitted radar signal is a function of the effective backscattering of all the targets that are present in a certain unit volume V_{res} of air at a certain distance (range) from the radar. For meteorological purposes these targets or scatterers are precipitation particles (hydrometeors) consisting of liquid water, for example rain, hail or snow. The returned power is usually expressed as the more familiar *radar reflectivity factor* Z with units $\mathrm{mm^6\,m^{-3}}$, referring to the sum of the diameters (to the power six) of all the scatterers in a volume. Reflectivity can thus be interpreted as an estimate of the amount and size of the different hydrometeors in the resolution volume of the radar. If the diameter of the hydrometeors is much smaller than the wavelength of the radar, Rayleigh scattering theory can be applied to calculate the radar reflectivity. Again see Appendix A for a more extensive derivation of the radar reflectivity factor Z.

Due to the wide range of values that Z can cover, reflectivity is often given in decibel units

db$Z$ where db$Z \equiv 10 \log_{10} Z$. High db$Z$ values appearing on a radar image are called radar echoes. Typical values of db$Z$ are 0-10 in drizzle or very light rain and 10-30 in moderate rain and up till 60 in moderate to heavy rain (Houze 1993).

3.1.1 Radar reflectivity: Rayleigh versus Bragg scattering

In an ideal case, all of the backscattered signals from clouds come from liquid water drops, *i.e.* ideal Rayleigh scattering. The reflectivity η of the backscattered signals is then given by:

$$\eta = \frac{\pi^5 |K|^2}{\lambda^4} \sum D^6 \tag{3.1}$$

where $|K|^2$ is the dielectric factor for water (0.93), λ is the wavelength of the radar signal and D is the diameter of a scatterer (Appendix A).

However, another source of radar backscattering are index-of-refraction variations in the air, called Bragg scattering. These variations arise from incomplete turbulent mixing in clear air between interfaces with different refractive indices, which are from humidity and temperature variations. If the turbulent fluctuations occur in the inertial subrange of isotropic turbulence (obeying the $k^{-5/3}$ law), at a scale close to $\lambda/2$, the radar signal will be scattered and the returned (Bragg) reflectivity is given by:

$$\eta = \frac{0.38}{\lambda^{11/3}} C_n^2 \tag{3.2}$$

where C_n^2 in m $^{-2/3}$ is the refractive index structure constant.

These echoes are often called clear-air echoes, because they are frequently observed in optically clear air. Values up to 0 db$Z$ for a 10 cm wavelength are often observed. Studies have shown that Bragg scattering also occurs in the early stages of a cloud. Especially at the top and edges of a cloud, turbulent mixing between moist and dry air produces Bragg reflectivities (the so-called mantle echoes), as long as this occurs at scales close to $\lambda\backslash 2$. Bragg scattering can also be observed at the trade-wind inversion or the transition layer.

A reflectivity factor of -20 db$Z$ might come from Rayleigh (hydrometeor) scattering in a cloud with droplets of 20 μm in diameter, but could also arise from Bragg scattering with a structure constant C_n^2 of 3.13×10^{-13} m $^{-2/3}$ for a radar wavelength of 5.49 cm. From Equation 3.2 it is clear that the Bragg scattered radar signal changes with wavelength. A 10 cm wavelength can give an approximately 10 db$Z$ stronger signal than a 5 cm wavelength radar for $C_n^2 \approx 5 \times 10^{-13}$ m $^{-2/3}$.

The S-Band wavelength is particularly sensitive to raindrops, because the diameter of raindrops (10^2 - 10^4 μm) is much smaller than the radar wavelength. Consequently, Rayleigh scattering theory can be applied to the backscattered signals to calculate the radar reflectivity Z. The large wavelength, however has a big disadvantage: S-Pol is very sensitive to Bragg scattering. Its big advantage is the low attenuation of the signal by intervening heavy rainfall and water vapor. In addition, S-Pol has the ability to measure reflectivity at both horizontal and vertical polarization (dual-polarization radar). Although not used in this study, this can provide useful information about the spherical properties of the

precipitation particles, helping to identify the development of very large hydrometeors. The K-Band wavelength is very effective in measuring the smaller cloud droplets ($\sim$ 10 μm) and is less sensitive to Bragg scattering, but its beam is attenuated by intervening rainfall.

It is desired to distinguish Rayleigh from Bragg scattering, especially if radar echoes result from Bragg scattering in clouds during their early development. The signal might then be falsely interpreted as arising from raindrops. A very good and extensive explanation of Bragg scattering and methods to distinguish between Bragg and Rayleigh are given by Knight and Miller (1993, 1998). One technique involves the use of a radar with two wavelengths, whereby one wavelength is usually less sensitive to Bragg scattering. The S-Pol radar for example has this advantage while it is equipped with both S- and K-band. Consequently, the difference in returned reflectivities between S- and K-band (as calculated with Equation 3.2) could be used to detect Bragg scattering.

3.1.2 Selection of surveillance scans

During the operational phase of RICO the S-Pol radar performed three types of scans: the Planned-position indicator (PPI) scan, the Range-height indicator (RHI) scan and the surveillance (SUR) scan. The PPI scans are made for a 120° sector and data is collected at up to 12 different elevation angles roughly every 4 minutes. This 120° sector was usually directed towards the general area of interest north of Barbuda, in the region of aircraft operations. A single RHI scan was made at the edge of a PPI sector from the lowest elevation to 90° upwards to retrieve routine information about the trade-wind inversion (Rauber et al. 2004). Surveillance scans with a full 360-degree rotation were made approximately every 20 minutes at the lowest elevation angle (0.5°) with scan rates of 8° s^{-1}.

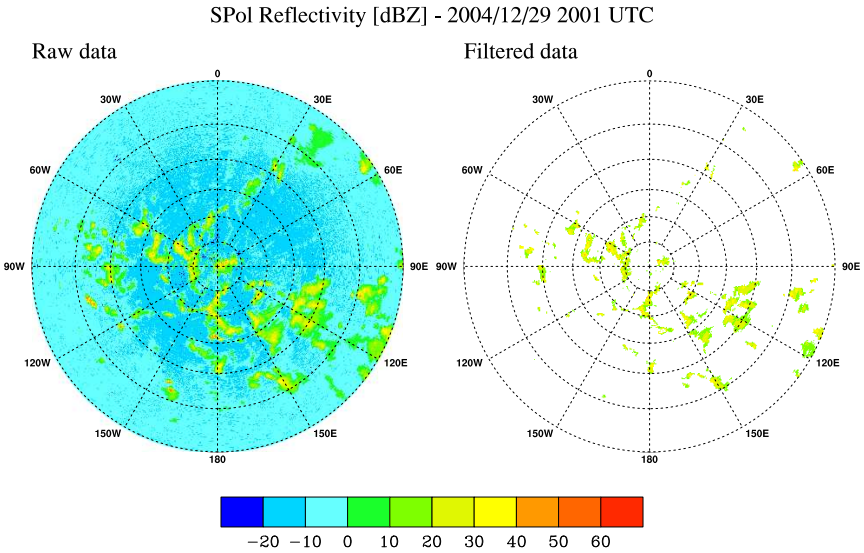

Figure 3.1: Radar echoes from shallow cumulus clouds appear on a surveillance scan of Dec 29, 2004 in both raw radar data (a) and filtered radar data (b). The range interval is roughly 25 km.

In this research only the surveillance scans are used since we are interested in gathering precipitation estimates at the largest scale possible. The radar pulse repetition frequency (PRF) was $1000Hz$, which limits scans to a maximum radius of 150 km. The 0.5° angle probes the atmosphere at heights below cloud top even at a large distance from the radar.

In Figure 3.1(a) an example of a surveillance scan is shown for a typical day (Dec 29, 2004) with shallow cumulus clouds. A wide range of db$Z$ values is observed, but the real echoes have reflectivities within 0 - 40 db$Z$. Blue areas have negative db$Z$ values, *i.e.* reflectivity factors Z smaller than 1 $mm^6\,m^{-3}$, and likely indicate Bragg scattering from clear air.

The actual period in which the radar operated included 66 days (November 21st - January 25th). For this period surveillance scans were selected with a 20-minute interval, resulting in approximately 70 scans a day. For every radar scan the reflectivity and velocity data were regridded into 'polar grid boxes'; each grid box or pixel having a range and azimuth interval of 150 m and 0.67 ° respectively. This resulted in a total of 540 (azimuth intervals) × 984 (range intervals) pixels per scan.

Due to beam broadening with increasing distance from the radar, the reflectivity, or rainfall intensity, will be increasingly underestimated and the areal coverage of echoes will be overestimated. This beam filling is likely to be the main reason for the gradual decrease in reflectivity with distance from S-Pol as shown in Figure 3.2 for the range beyond 20 km. In this figure, the reflectivity for all scans, averaged over all azimuth angles, is plotted against range. Another reason for the db$Z$ attenuation with range may be the increasing beam axis altitude, whereby the radar beam will be partly located higher in the cloud beyond a certain range. It is not very likely that attenuation of the radar beam, due to scattering and absorption by clouds and intervening heavy precipitation, will have a significant effect at this wavelength. The sharp increase in db$Z$ for the range below 20 km may indicate that part of the precipitation evaporates before reaching the surface or even the lower part of the atmosphere.

The different impact of these artifacts is not well understood and it is desired to exclude as many unknown errors as possible. Therefore, based on Figure 3.2, a smaller domain between 20 - 60 km, in which the average db$Z$ value remains roughly constant, is chosen for further analysis. This reduces the total number of pixels to 540 × 267.

The height of the radar beam axis (plotted on the second x-axis) that corresponds to these range limits is 170 m and 520 m respectively. Keeping in mind that trade-wind cumulus clouds have an average cloud base height of 500 - 1000 m ((LeMone and Pennell 1976; Neggers 2002; Stevens 2005), it can be assumed that the radar beam is located below the clouds. Therefore, the precipitation particles measured will already be falling from the cloud toward the surface. This is useful to keep in mind when interpreting the reflectivity values in the following results. However, from the horizontal scans no detailed information can be obtained about their exact location and whether the particles reach the surface or not.

3.1.3 Error estimates and data filtering

Beside the range attenuation mentioned in the previous section, radar measurements are subject to many errors which are sometimes difficult to detect and even harder to estimate. For the purpose of this study it is not desired to do so, although errors will be discussed

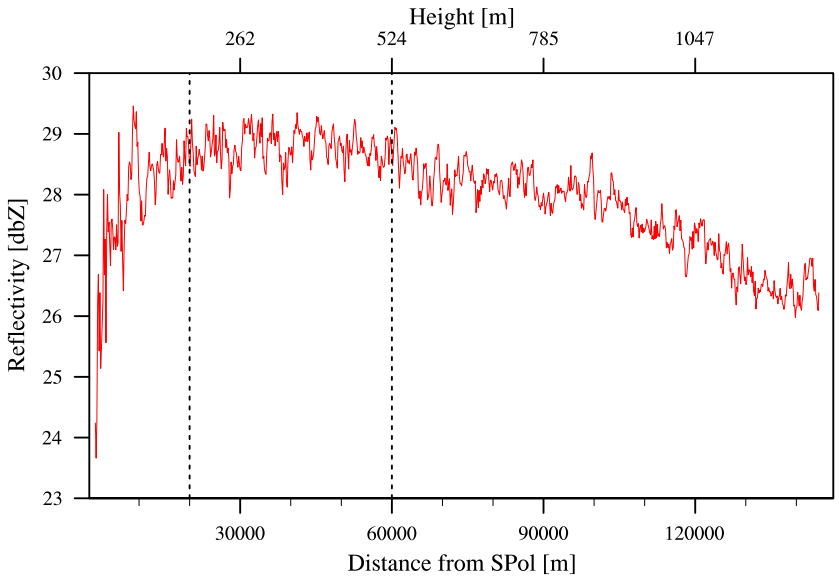

Figure 3.2: The radar reflectivity in db$Z$ is averaged over all azimuth angles and plotted against distance from the S-Pol radar and height of the radar beam above the surface. The dashed lines at a 20 and 60 km distance indicate the domain that is selected for further analysis.

and filtering methods are applied to improve the quality of the dataset. Nevertheless, the reader should keep in mind at all times that the type of analysis done here is aimed at retrieving relative amounts of precipitation rather than absolute amounts. Quantitative values in the results should not be given too much emphasis.

One of the errors is a correction of +1.4 db$Z$ in the calibration, due to hardware problems, that is not yet applied to this dataset. Rather negligible are errors due to the spatial and temporal variation in (rain) drop size distributions (see the next section 3.1.4: from reflectivity to rain rate). An unwelcome effect in transmitted radar signals is anomalous propagation (AP). This is abnormal propagation due to differences in density or refractive index of the atmosphere, resulting in unusual reflections that can cause false echoes to appear on a radar image. Examples of AP are ground clutter (beam blockage) and sea clutter. Ground clutter is backscattering from objects such as vegetation or rocks. These objects cause the side lobes of the radar beam to be refracted downwards to the surface or to be blocked at a low elevation close to the radar. The islands in the RICO area (among which Antigua and Barbuda) produced ground clutter. Sea clutter occurs at times with strong winds when scattering of the radar beam by ocean waves produces weak reflectivities.

In this analysis an effort is made to detect false echoes due to clutter and filter them in the best possible way. In addition, the clear air echoes indicating Bragg scattering are excluded by a masking technique, so that all the remaining radar echoes represent merely rain from clouds. The filtering and masking techniques are applied in the following order: 3.1.3.1) Island filtering, 3.1.3.2) Bragg scatter filtering and 3.1.3.3) Sea clutter filtering.

3.1.3.1 Island filtering

The pixels suffering from ground clutter were identified by averaging the reflectivity values of all the available scans during the whole period for every pixel. The reflectivity histograms for pixels located above an island (not shown) were skewed to very high values (above 40 db$Z$), whereas pixels above the ocean were skewed toward values below 0. Pixels with an average reflectivity higher than 0 db$Z$ were therefore labeled as island pixels and set to missing values. In Figure 3.1 for example, pixels in the center of the scan (the island Barbuda) appearing as yellow and red in 3.1(a) have disappeared in 3.1(b).

3.1.3.2 Bragg scatter filtering

In Figure 3.3(a) we plot the histogram of reflectivity (db$Z$) and zoom in, in Figure 3.3(b), to show the distribution of the higher reflectivities. In this histogram the reflectivity values of pixels for all surveillance scans were counted. The high percentages at values below 0 db$Z$ are primarily the result of Bragg scattering and noise (seen before as the extensive blue areas on the radar image in Figure 3.1 a)).

Although in 3.3(a) reflectivities above 10 db$Z$ seem to be rare, 3.3(b) shows this is not the case. The transition at 0 db$Z$ from a sharp to a smooth decrease indicates that this histogram is likely a combination of two different histograms: of Bragg scattering and Rayleigh scattering. Despite the transition at 0 dBZ, the two cannot easily be distinguished at low reflectivities (-10 to +10 db$Z$) if only S-band is used. Unfortunately, the K-band data for the 0.5° angle was very sensitive to beam blockage, caused by the low bushes (z $\approx$ 1.5 m) surrounding the radar site at Barbuda. K-band is therefore not a reliable data source for the horizontal statistics and for detecting Bragg scattering. Knight and Miller (1993) studied the transition from Bragg to Rayleigh scattering and concluded that for S-band above 10 db$Z$ the radar signal can be assumed to arise from almost only precipitation. For this reason Bragg scattering is eliminated by using this 10 db$Z$ cut-off value; all the reflectivities in the dataset below 10 db$Z$ are masked. As a consequence, part of the Rayleigh scattering may be masked in this dataset as well.

3.1.3.3 Sea clutter filtering

After both island and Bragg scatter filtering was applied, several pixels with unusual high reflectivities appeared on the radarscans at distances close to the radar, representing sea clutter. On several scans the amount of sea clutter was considerable, leading to the decision to filter these pixels as well.

When observing cross sections through various azimuth angles, it was found that high reflectivities associated with sea clutter are often accompanied by unusual (high or low) radial velocity values. This information was used to set pixels that deviated more than half a standard deviation from the average radial velocity for a certain azimuth to a missing value. Unfortunately, the assumption that sea clutter pixels have an unusual radial velocity does not always hold. Many sea clutter pixels still remain included when only this filtering technique is applied.

It was also observed that sea clutter often appears as a single isolated pixel, whereas a real echo usually consists of more than one pixel. Therefore, an additional filtering technique was applied where pixels not surrounded by other pixels with a high reflectivity were

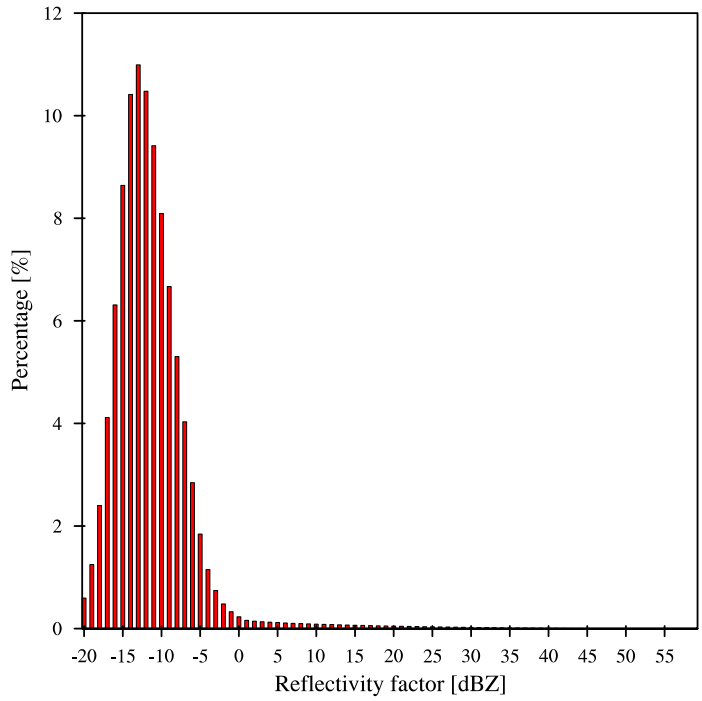

(a)

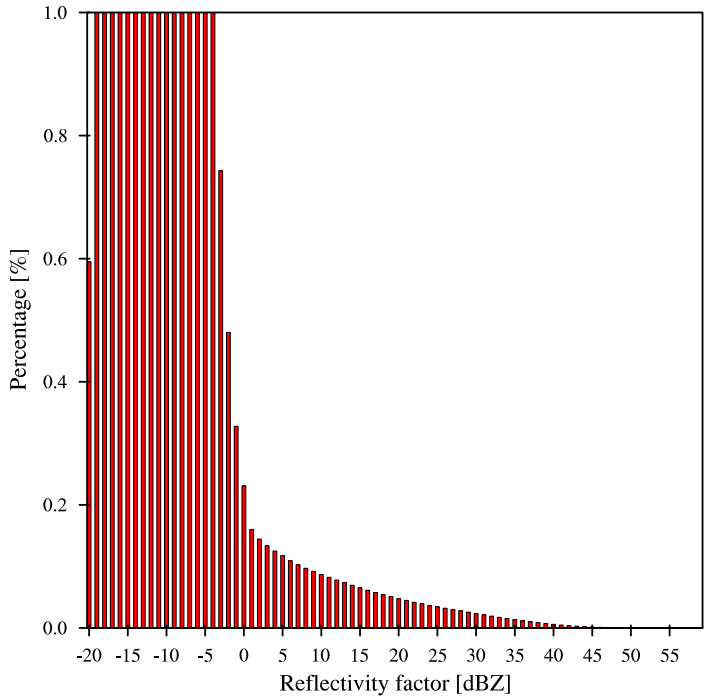

(b) Zooming in at histogram (a)

Figure 3.3: Histograms of reflectivity (db$Z$) for all S-Pol radar surveillance scans during the operational phase of RICO

set to missing values. This was achieved by creating four new polar maps, each having data regridded in a slightly different way. Namely, the data for each pixel was either shifted to the next pixel in range, or to the previous pixel in range, or to the next or previous pixel in azimuth. By overlying the original map with one of the new maps, the data of the new map could be substracted from the original data and for each pixel the resulting deviation was squared. This was done for each of the new maps, resulting in four comparisons, and thus four squared deviations for each original pixel. These four squared deviations were summed and plotted on the original map, on which values ranging from zero to five hundred and even higher could yet be observed. The pixels with an exceptional high value indicated that they had been surrounded by values much less than their own, raising the possibility they represented a sea clutter pixel. These pixels could be easily identified and filtered in addition to the first described method.

After filtering it is assumed that all the echoes left in the data are real echoes, *i.e.* precipitation. An example of filtered data is shown in Figure 3.1(b). The echoes in this scan are large in diameter, sometimes reaching 20 km or more. They could be described as rain bands in a clustered cloud field. Some isolated echo cells smaller than 3 km in diameter can be seen as well.

3.1.4 From radar reflectivity to rain rate

Radar reflectivity Z is related to the size of the scattering particles. More specifically, Z is related to the sixth power of the (rain) drop size distribution (see equation 5.5). Because the rainfall rate (R) is a function of the diameter of the particles as well (equation 5.6), the two are empirically related by a reflectivity - rain rate (Z - R) relationship. This relationship is usually written in the following form:

$$Z = \alpha R^{\beta} \tag{3.3}$$

with R in mm h^{-1} . Coefficients α and β depend on the location and the season, but not on the rain rate itself (Houze 1993; Steiner et al. 2004; Uijlenhoet 2004).

Warm rain showers, *i.e.* no ice particles involved, are known to develop by a process of coalescence of water (cloud) droplets due to their different fall velocities, whereby the largest droplets act as the collectors. The origin of these collector droplets still remains controversial. The coalescence process results in a large number of cloud droplets formed relatively close to the cloud base that rain out early. All the different processes in a cloud (coalescence, break-up, evaporation etc.) affect the rain drop size distribution and determine the type of $Z - R$ relation that should be used (Rosenfeld and Ulbrich 2003).

An extensive analysis of the processes determining the coefficients of a $Z - R$ relation for trade-wind clouds is beyond the scope of this study. In addition it is assumed that the large number of scans and the scale of the RICO area studied will average out spatial and temporal variations.

Hundreds of different $Z-R$ relations have been reported during the past decades. Relations exist for different cloud types, for different backgrounds (continental, maritime), for various heights and places in the cloud (cloud base, cloud top or cloud core) and so on. These relations are the result of extensive studies on observed drop size distributions and rain

rates at different climatological locations. For example, studies have provided adequate relations for moderate to heavy rain in deep-convective and stratiform regions in mesoscale convective systems (MCS's) over tropical oceans (Tokay and Short 1996) and also for drizzle in maritime stratocumulus (Van Zanten et al. 2005).

However, no analysis of in-situ observations of radar reflectivity and drop size distributions has provided a Z - R relation specifically for the trade-wind clouds. Therefore in this analysis a relation is used for warm rain showers in general. The coefficients are derived by Uijlenhoet (2004) as the mean value of six relations for warm rain showers as reported by Battan (1973):

$$Z = 248R^{1.75} \tag{3.4}$$

In comparison, for the space born Tropical Rainfall Measuring Mission (TRMM) precipitation radar, the Z - R relation used for shallow and deep convection is $Z = 148R^{1.55}$ (TRMM PR Instruction Manual 2004). A relation for drizzle from marine stratocumulus was derived from drizzle observations near the surface during the DYCOMS-II field study: $Z = 7.25R^{2.94}$, here with R in mm day^{-1} instead of mm h^{-1} (Van Zanten et al. 2005).

Using Equation 3.4 every radar pixel was converted to a rain rate. For the purpose of this study it was desired to estimate rainfall in the whole area covered by the radar, instead of analyzing the rain rate at a single location. After applying Eq. 3.4 three important variables were derived for every radar scan to provide this sort of information: the *echo coverage*, the *area rain rate* and the *echo rain rate*.

The *echo coverage* $F(R_\tau)$ in percent was calculated as an expression for the fraction of the area (within a 20 - 60 km range) with rain above the threshold τ of 10 db$Z$ ($R_\tau \approx 0.15$ mm h^{-1}):

$$F(R_\tau) = \frac{A(R_\tau)}{A_T} \times 100 \tag{3.5}$$

where $A(R_\tau)$ is the number of pixels with $R > R_\tau$ and A_T the total number of pixels in a scan.

Consequently, an *echo average rain rate*, R_{echo}, was calculated with only pixels above the threshold τ included. The sum of rain rates $> R_\tau$ in a scan was divided by $A(R_\tau)$:

$$R_{echo} = \frac{\sum R}{A(R_\tau)} \tag{3.6}$$

This can be considered as a conditional rain rate. Finally, an (unconditional) *area average rain rate*, R_{area}, was calculated by dividing the sum of rain rates $> R_\tau$ in a scan by A_T:

$$R_{area} = \frac{\sum R}{A_T} = R_{echo} \times F(R_\tau) \tag{3.7}$$

3.2 Rain gauge and satellite remote sensing data

To verify rain rates estimated with the radar reflectivity data, other data from rain gauge measurements and satellite remote sensing are used in this study as well. The rain gauge

was located at the Integrated Surface Flux Facility (ISFF) meteorological station at Barbuda (17°33.047' N, 61°44.259' W), where rain rates (5 minute statistics) were collected in the period of December 3rd (2004) - January 25th (2005). These measurements may have been influenced by high winds affecting the collection efficiency of the tipping bucket, resulting in a lower accumulation of rain. Other instrumentation at this surface station included a RMYoung Propellor Vane at 10 m, Vaisala 50Y Humitters at 2 m to measure air temperature and relative humidity and long and short wave radiometers. All the measurements are 5-minute averages.

Rainfall estimates from satellite remote sensing includes the daily precipitation data from the Global Precipitation Climatology Project (GPCP), derived from infrared and passive microwave radiances measured by a geostationary satellite. The $1^\circ \times 1^\circ$ grid box chosen for this study is centered at Barbuda and corresponds roughly to a 100×100 km area. These rain rates are available for each day during RICO.

Other rainfall estimates are derived from the space-borne TRMM precipitation radar (PR). One TRMM orbit around the Earth is completed in 91 minutes, resulting in 16 orbits per day, that can be used to map rainfall in the tropics. This precipitation radar on board of the TRMM satellite can directly observe vertical distributions of rain. The PR antenna beam scans in cross-track direction over $\pm$ 17°, making a 220 km swath width from end to end, with 49 observation angle bins of 0.71°. The horizontal resolution is 4.3 km at nadir and the range (and thus vertical) resolution is 250 m. Radar echo sampling is performed from sea level up to an altitude of 15 km. For this study 17 TRMM orbits were selected during the RICO period in which the PR antenna beam axis was centered close to the Caribbean islands at the location of the field study. From these scans only the rainfall data at the surface was used as comparison to the S-Pol time series of rainfall.

Chapter 4

Results and discussion

4.1 Reflectivity histogram for shallow cumulus

In Figure 4.1 the histogram of reflectivity is shown for the filtered radar data. This is essentially the same histogram as shown in Figure 3.3 in Chapter 3, but for values above the threshold of 10 db$Z$ and after sea and ground clutter are filtered. One important difference with the raw data histogram is that reflectivities between 10 and 20 db$Z$ have a lower percentage, *i.e.* occur less often, than reflectivities of $\sim$ 20 db$Z$. This is remarkable, because in Figure 3.3(b) the percentages below 20 db$Z$ are higher compared to percentages at $\sim$ 20 db$Z$. This appears to be an unwelcome consequence of one of the sea clutter filtering methods. With this method single isolated high reflectivity pixels, not surrounded by other pixels with a high reflectivity, were set to a missing value. This implies that pixels at the edge of a real cloud echo, at the transition from a reflectivity above 10 to one below 10 db$Z$, may be falsely labeled as sea clutter. Consequently, the filtering method is cutting at the edges of the real echoes, that are often marked by reflectivities below 20 db$Z$. This results in less pixels with values in between 10 - 20 db$Z$, while the number of pixels with reflectivities of 20 db$Z$ and higher remain relatively unchanged.

This histogram represents precipitation from the shallow cumulus clouds observed during RICO, as fields of trade-wind cumulus, cumulus congestus, lines of cumulus and cloud clusters. Although information about the vertical cloud structure, for example cloud depth, is not given in detail in this report, it is known from weather and flight reports that most days during RICO were characterized by these shallow clouds (see also paragraph 2.3). The mean reflectivity of this histogram is 23.1 dBZ. In comparison, the mean value of the deep convective clouds in mesoscale cloud systems (MCS) occurring above the tropical oceans is 38.0 db$Z$. The stratiform tail of the MCS's have a mean value of 30.2 db$Z$ (Tokay and Short 1996).

More than 50% of the echoes studied during RICO have reflectivities above 21.0 db$Z$ and still 10% is above 32.5 dBZ, as shown in Table 4.1 in which the accumulative percentages are given. Also given are the corresponding rain rates based on three different Z - R relations. The first one is used in this study (Equation 3.4), the other two are given as a comparison (for the TRMM precipitation radar and DYCOMS-II study respectively, see section 3.1.4). Z - R relation 1 and 2 are quite similar and give comparable results. The third relation gives rather different results, which might reflect the fact that this relation is based on the observed distribution of drizzle drops from stratocumulus during the

DYCOMS-II field study. It is clear that with the use of another Z - R, very different rain rates can be obtained. However, if a rain rate higher than 1 mm day^{-1} is already considered to be heavy drizzle (Van Zanten et al. 2005), regardless of the Z - R used, the clouds observed during RICO are producing at least heavy drizzle and sometimes even light or perhaps moderate rain.

4.2 Area rainfall during the RICO field study

4.2.1 Time series of rainfall and winds

For each radar scan an area rain rate R_{area} and echo coverage were determined and plotted in a time series for the operational period of S-Pol during RICO. These variables are shown in the two top plots in Figure 4.2. The time in UTC is the local time on Barbuda plus 5 hours.

From Figure 4.2 it is clear that the rain rate coincides to a high degree with the coverage. This indicates that the overall area rainfall depends largely upon the coverage of the precipitating clouds. It suggests that the intensity of the rain varies little over the area or that peak events of localized heavy rain have a small influence on the total area rain.

The time series shows much variety in the amount of rainfall during RICO and several relatively wet or dry periods can be distinguished. The whole latter part of November was a dry period with suppressed conditions. The period at the end of RICO, starting around January 20$^{\text{th}}$, was a dry period as well. A measure of the actual intensity of the rain R_{echo} is the echo reflectivity in dBZ, shown in the third plot of the time series. This echo reflectivity is averaged over 6 hours. The reflectivity is about 2 - 4 db$Z$ lower in the dry periods at the start and end of RICO. At the end, the reflectivity even drops substantially in a short period. This drop happens shortly after a change in wind direction and drop in wind speed and relative humidity, indicating the advection of dry subtropical air into the area. The winds and relative humidity are shown at the bottom plots in the time series as hourly averages of measurements done at the ISFF surface station. The standard deviations are given in blue. The interpretation of the humidity should be taken with caution, because of the possibly large influence of the surface (the measurement height is 2 m). The incoming longwave radiation at the bottom plot may serve as an indication of cloud cover, with larger incoming radiation corresponding to more clouds. Unfortunately, no surface measurements are available during the first dry period.

The relatively wet period by itself, from the beginning of December to January 20$^{\text{th}}$, can be further subdivided. Two periods of heavier rain stand out, the first on the 12$^{\text{th}}$ - 14$^{\text{th}}$ of December and the second on the 9$^{\text{th}}$ and 13$^{\text{th}}$ of January. The weather reports indicate that during the heavy rain days in December, moist convection from the (sub)tropics and an unstable atmosphere resulted in deep convection. Deep convection was also triggered by a gust front. Research flights during this period were avoided as much as possible. After these rainy days, a relatively dry period started. Yet this period was marked by several smaller rain peaks as well. Characteristic for the trade-wind region were the typical fair weather conditions during this dry period, with winds coming persistently from the east - northeast. On January 9$^{\text{th}}$ a strong surface trough was present with extensive cloud cover, related to the second heavy rain event. Another peak in area rainfall occurred on

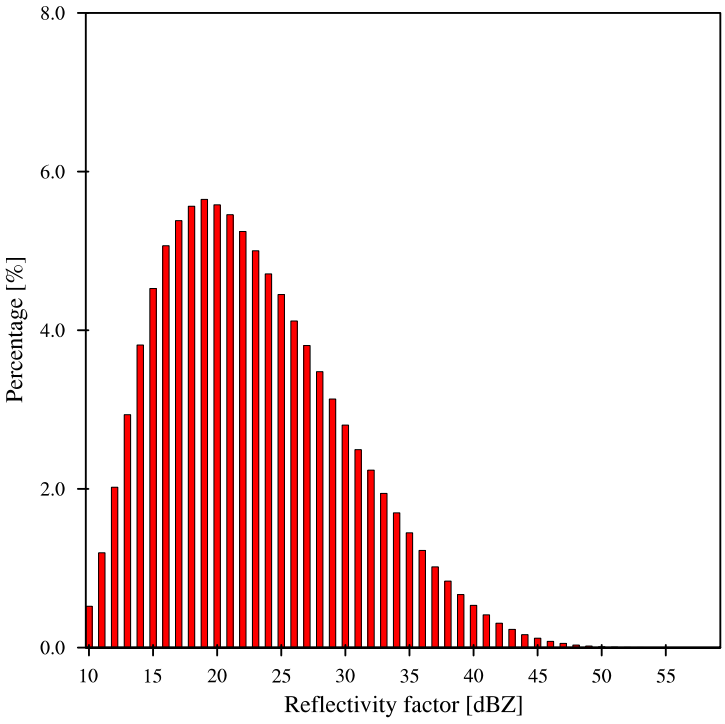

Figure 4.1: Histogram of reflectivity (db$Z$) for shallow cumulus in the trade-wind region observed with the S-Pol radar during the RICO field study. Reflectivity values are counted for all pixels in all available surveillance radar scans after data filtering is applied (see also Chapter 3).

Accumulative percentage [%]	**Z** [db$Z$]	**R** [mm h^{-1}]		
		1)	2)	3)
10	13.5	0.253	0.296	0.061
25	16.5	0.375	0.462	0.077
50	21.0	0.679	0.912	0.110
75	26.5	1.40	1.880	0.170
90	32.5	3.082	4.140	0.271

1) $Z = 248R^{1.75}$ - Uijlenhoet (2004)
2) $Z = 148R^{1.55}$ - TRMM PR Instruction Manual (2004)
3) $Z = 7.25R^{2.94}$ - Van Zanten et al. (2005)

Table 4.1: Accumulative percentages of reflectivity values based on the histogram for shallow cumulus in Figure 4.1. Rain rates calculated using three different Z-R relations are also given, see also section 3.1.4.

January 13th when easterly surge bands moved through the RICO area. The rainy period in January was ended with the passage of a cold front on January 19th, recognized in the time series by the change in wind direction and drop in wind speed.

4.2.2 Probability of rainfall

Although the period in between the heavy rain events can be considered relatively dry, there are still many small rain rate peaks visible. These peaks are associated with typical shallow cumulus clouds, known from observations during RICO. All these small rain events contribute significantly to the total rainfall observed by S-Pol. To be more precise, 50% of the total rainfall (97.6 mm in 66 days as derived from the radar data) is produced by clouds with an average daily area rain rate (R_{area}) below 0.125 mm h^{-1} . This is shown in the cumulative probability of rain plotted in Figure 4.3. The cumulative probability is approximated by taking the sum of the daily averages of area rainfall and dividing it by the total rainfall. In the time series of rainfall, almost all the smaller rain peaks occur below this value of 0.125 mm h^{-1} . Although no confident statement can be made on the exact quantitative rain rates, these first estimates may indicate the precipitation from shallow clouds is much more important than previously assumed.

The average R_{area} and echo coverage for the whole RICO period were 0.72 mm day^{-1} and 1.72 % respectively. An average R_{area} of 0.72 mm day^{-1} is quite high, compared to the previously reported monthly average rainfall of 9.7 mm produced by shallow storms over the whole tropical ocean regions by using the TRMM precipitation radar data (Short and Nakamura 2000). If all the rainfall contributing to the above mentioned 50% would in fact come from shallow cumulus, then its contribution to the total rainfall over this part of the trades is certainly not negligible.

4.2.3 Comparison with surface and satellite rainfall estimates

The time series of rainfall is compared to other rainfall estimates from the ISFF surface station on Barbuda, the TRMM precipitation radar and the GPCP precipitation analysis (see also paragraph 3.2). These are plotted in Figure 4.4, together with the S-Pol derived rain rate from Figure 4.2. The rain gauge data from the surface station, in blue dots, are 2-hour averages and should be interpreted as relative rain rates. They are more useful for the comparison of relative amounts of rainfall than for absolute rain rates. TRMM and GPCP rain rates, both daily average rain rates, are given in red and grey bars respectively.

The surface rain rates coincide surprisingly well with S-Pol rain rates, especially if one recalls that the surface station is not even located in between the range of the data selection (starting at the range of 20 km). The total rainfall measured with the rain gauge during a 53 day period was 49.7386 mm. Some of the heavy S-Pol rain peaks are missing in the surface rain rates, for example on December 15th. However, many of the small rain peaks (see for instance Dec 19th - 23rd and Dec 29th - 31st) are present in the surface time series. This suggests the precipitation actually reaches the surface in many cases. The S-Pol area rain rates may thus be a good representation of the local precipitation at the surface.

As can be expected from the horizontal resolution and the rainfall estimate methods used in the GPCP analysis, none of the small rain events are detected. On a 100 km $\times$ 100 km scale, the shallow cumulus clouds are overlooked and only higher and bigger clouds are

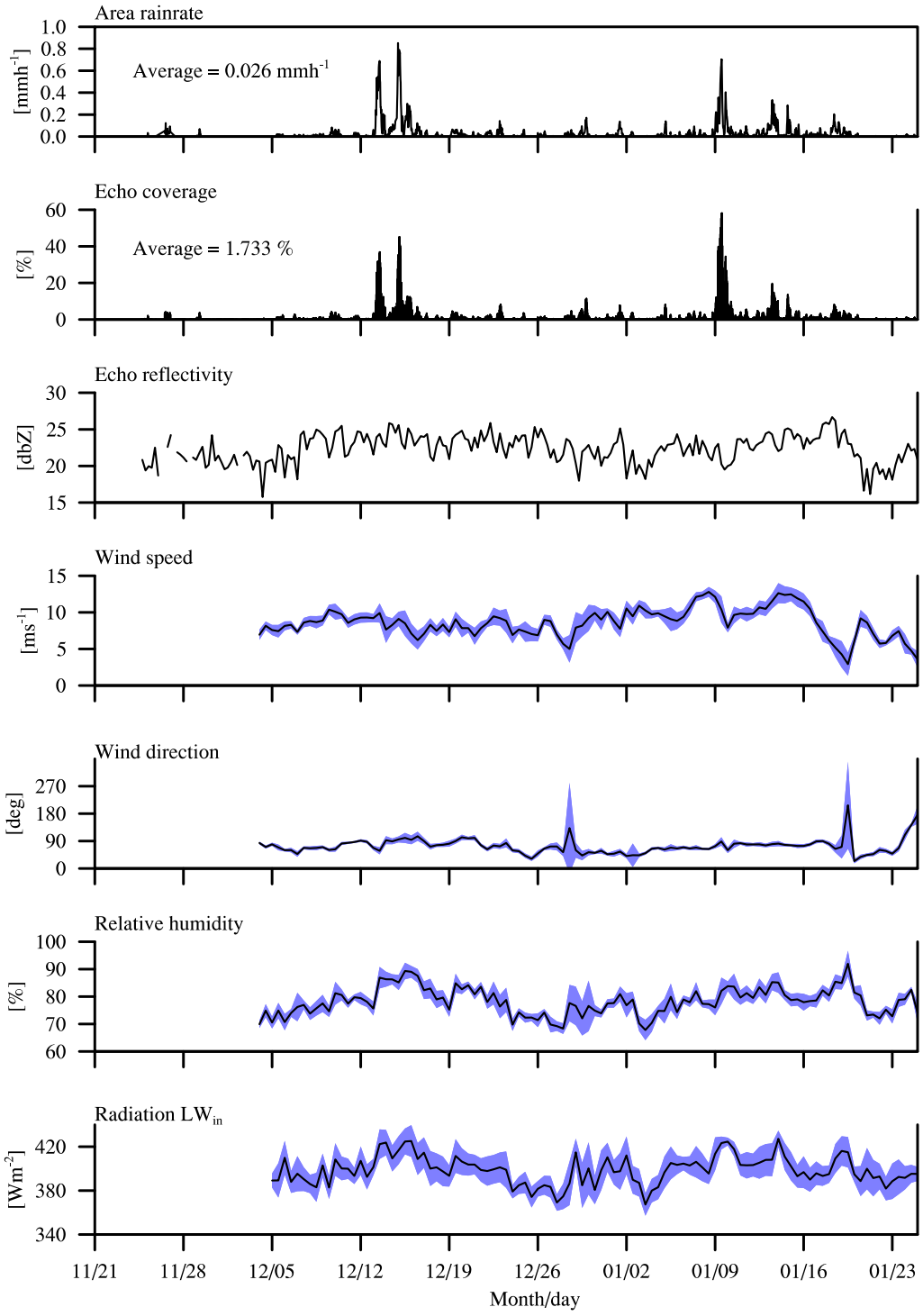

Figure 4.2: Area rain rate (mm h^{-1}) and echo coverage (%) for each radar scan plotted against date (UTC) during the RICO operational period (2004/11/21 - 2005/01/25). Echo reflectivities (db$Z$) represent 6 hour averages. Wind speed (m s^{-1}) and direction (deg), the relative humidity (%) and radiation (W m^{-2}) all represent hourly averages measured at the ISFF surface station. Given in blue are the standards deviations.

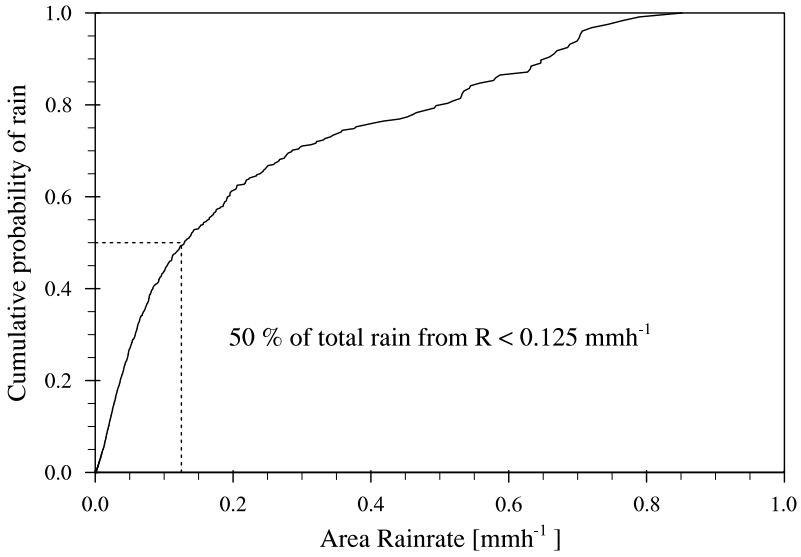

Figure 4.3: The cumulative probability of rain is plotted for the daily average area rain rate, that is derived from S-Pol radar data.

detected in the infrared and microwave channels and associated with precipitation. The total rainfall in 66 days is estimated as 150.323 mm by GPCP, which in turn would imply an unrealistic high average rain rate (2.27 mm day^{-1}).

Unfortunately there are just a few TRMM overpasses for the RICO area and thus this data is not very useful for a (relative) rainfall comparison. Nevertheless, on the days for which the overpasses are available, rainfall occurs at such significant rates that it can be observed from space by TRMM. Even in the dry month of November, some small red bars are present. TRMM has proven to be a successful instrument in mapping precipitation on a global scale and recently the ability of TRMM to indicate shallow precipitation has been the subject of several studies ((Short and Nakamura 2000; Lau and Wu 2003; Schumacher and Houze 2003a, 2003b)).

4.2.4 Area differences

Most of the research flights during RICO were conducted in the upwind area north - northeast of Barbuda. With the S-Pol data, it can be verified whether this location is representative for a larger area in the Caribbean. The S-Pol data was divided into a north, east, south and west area, each consisting of 180°. For each area and radar scan, rain rates and echo coverage were calculated and then averaged for all available scans during the operational period. These periodic averages are shown in Table 4.2. In addition, an upwind and downwind area of 10° each were determined. Based on the daily average wind direction, derived from the S-Pol radial velocity, the upwind and downwind area shifted each day.

There are no significant differences in coverage and rain rates between north and south, or between east and west. The echo rain rate (R_{echo}) tends to be sensitive to the size of the area. The larger the area, the larger R_{echo}. This could be explained as follows: if the area is smaller, a precipitating cloud (cluster) is easily missed. If covered by a larger area, the

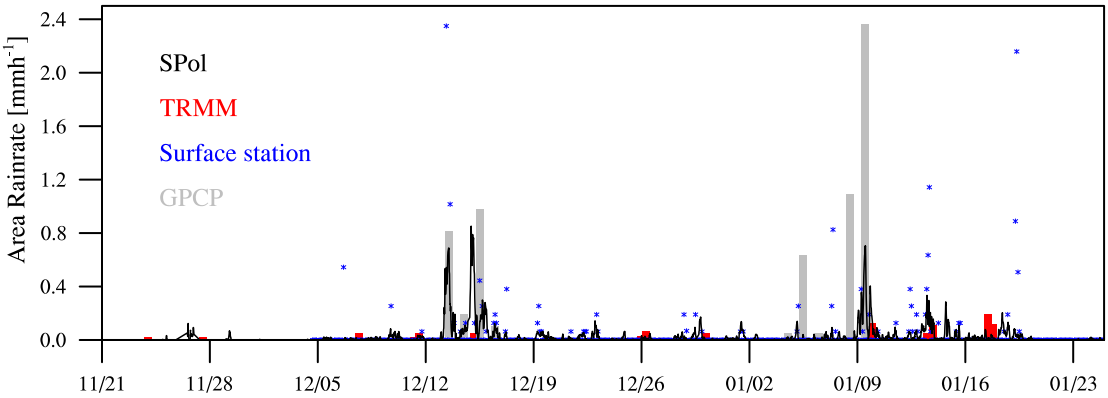

Figure 4.4: Rain rate estimates in mm h^{-1} are plotted for the RICO operational period (month/date). In black the same S-Pol derived area rain rate as in Figure 4.2 is shown. Blue dots represent the (relative) raingauge derived rain rate, here averaged over 2 hours for convenience. Surface area rain rates derived from 17 TRMM overpasses are given as red bars. The area rain rate derived from GPCP daily precipitation data for a $1° \times 1°$ grid box is shown in grey.

R_{echo} would increase substantially because it is a conditional rain rate. This effect would be smaller for the unconditional area rain rate.

The difference in upwind and downwind area, however, is not negligible. Rainfall apparently occurs more frequently upwind from Barbuda than downwind. This is an interesting result, if proven significant, for the student research, because evidence of a raining island tail downwind from Barbuda is apparently not obvious from these values. When the differences were studied day by day instead of the whole period at once, the presence of an island tail on satellite images did not corresponds systematically to a higher echo coverage (or rain rate) at the same day. Also, no differences between day and night were evident, which could have indicated the role of an island heating effect in the development of the tail clouds.

By observing the radar images of raw data, however, it was observed that an island tail can in fact be distinguished downwind, by a higher reflectivity than its surrounding air. But even these reflectivities are not higher than 0 - 10 db$Z$ and thus are filtered from the dataset. Reflectivities above 10 db$Z$ are usually only observed beyond a range of 80 km from S-Pol, and thus excluded from the dataset.

If the lifetime of a cloud can be determined by precipitation in any meaningful way, one interpretation of the smaller echo coverage downwind can be that the initiation of precipitation in the tail clouds takes a longer time. This could be caused by an increased amount of nucleation sites from aerosols, transported from the island. More insight into whether the tail clouds really precipitate, where this occurs and how this may influence their lifetime and the sudden end of the tail, needs more detailed analysis. This radar dataset can be very helpful in providing answers to these questions, if the area is extended and reflectivities below 10 db$Z$ are not filtered from the dataset.

Area [deg]	**Echo coverage** [%]	**Area rain rate** [mm h^{-1}]	**Echo rain rate** [mm h^{-1}]
total (360°)	1.73	0.026	1.332
north (180°)	1.70	0.026	1.202
south (180°)	1.76	0.026	1.292
east (180°)	1.74	0.028	1.239
west (180°)	1.72	0.025	1.256
upwind (10°)	1.69	0.028	1.187
downwind (10°)	1.48	0.019	1.218

Table 4.2: The echo coverage and rain rates averaged over the RICO period are given for different area's in the radar domain. The area size is given in degrees.

4.3 Daily differences in rainfall

4.3.1 Histogram anomalies within the RICO period

The days during RICO were sometimes very different with regard to the (relative) rainfall. Because area rainfall depends so much on the echo coverage (shown in Figure 4.2), it is not directly obvious how the actual intensity of the rain differs between days, if it differs at all. If one wants to select a case for a cloud study on a particular day, it is important to have an idea about whether a day is characterized by a few heavy precipitating clouds or by many small clouds with drizzle. The reflectivity values given in a histogram reveal more information on the actual rain intensities (echo rain rates) that occur.

Histograms were calculated for each day and then subtracted from the (general) histogram for shallow cumulus in Figure 4.1. The deviations from this histogram will be called (daily) histogram anomalies. The anomalies for six days spread over the RICO period are shown in Figure 4.5. The daily average echo coverages are shown as percentages in the graph. Remarkably are the two anomalies for December 14^{th} and January 9^{th}. Both days reach almost the same area rain rate in Figure 4.2, but apparently their actual rain intensity is very different. The histogram of December 14^{th} is skewed to higher reflectivity values, in agreement with the weather reports of a very unstable atmosphere with deep convective clouds and heavy rainfall. January 9^{th} has a histogram skewed to lower values that is approximately opposite to December 14^{th}. The large echo coverage, however, causes very high values for the area rain rates, despite low rain intensities (R_{echo}).

After December 14^{th}, histograms start gradually to look more like the shallow cumulus histogram. Not all the days after December 14^{th} are shown here, but the return to lower reflectivity values can be observed here from the difference in the anomalies for December 14^{th} and December 18^{th}. It is evident that days may differ much with regard to the actual rain rates occurring on them, at least more than the time series reveal. Taking only the time series into account when describing the rainfall characteristics of a certain day can therefore be misleading.

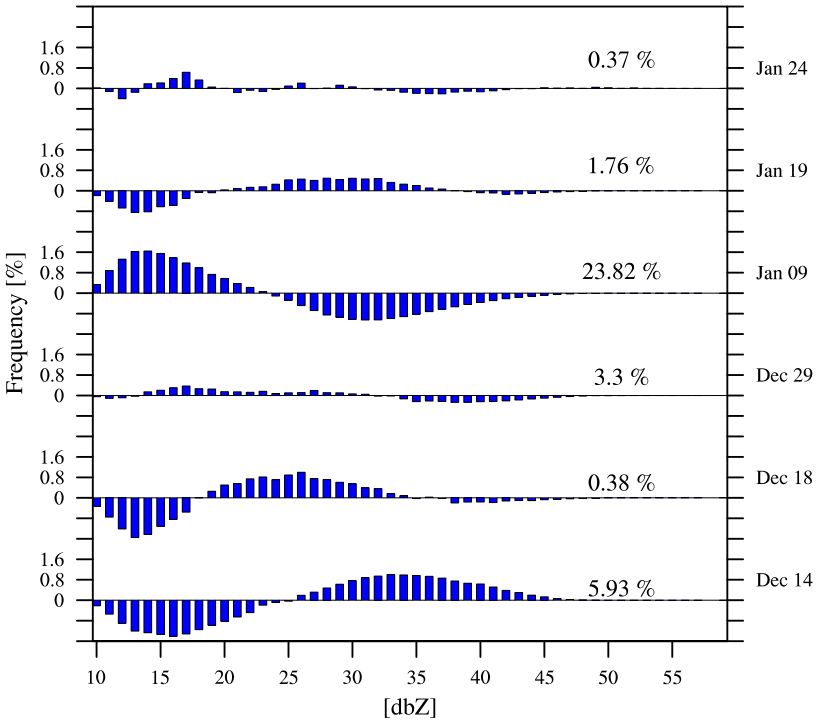

Figure 4.5: The histogram anomalies, *i.e.* deviations from the histogram for shallow cumulus in Figure 4.1, are shown for several days during RICO. Also shown is the daily average echo coverage.

4.3.2 Rainfall versus cloud (echo) type

At a certain point, it gets interesting to estimate the precipitation that is typical for just the shallow cumulus clouds in the trade-wind region. To achieve this, rain rates need to be related to cloud type. For example, it is interesting to identify whether a typical trade-wind cumulus cloud or a deeper cumulus congestus cloud produces a certain rain rate. Cloud types and their vertical structure can be described for example day by day, by using sounding data and photographs taken during the research flights.

It is desired to exclude days from the dataset that are not characterized by shallow cumulus. The histogram anomalies and the time series already reveal several days that should not be considered as typical shallow cumulus days. Here, some first very general criteria are applied to exclude those days. These criteria are defined partly by observing the time series and histograms and are applied to the daily averages of the rain rates and echo coverage.

At first, days with an area rain rate (R_{area}) higher than 0.1 mm h^{-1} are excluded. This value is chosen after analyzing the daily average values. Many of the days with a R_{area} higher than 0.1 mm h^{-1} can be identified in the time series by a significant peak in the amount of rainfall. However, these peaks do not automatically have to result in a high daily average. Consequently, by just using this criterion, a few days that should be excluded are not. Therefore another criterion is applied to account for this: days with an echo rain rate (R_{echo}) higher than 1.8 mm h^{-1} ánd a coverage higher than 2 % are also excluded.

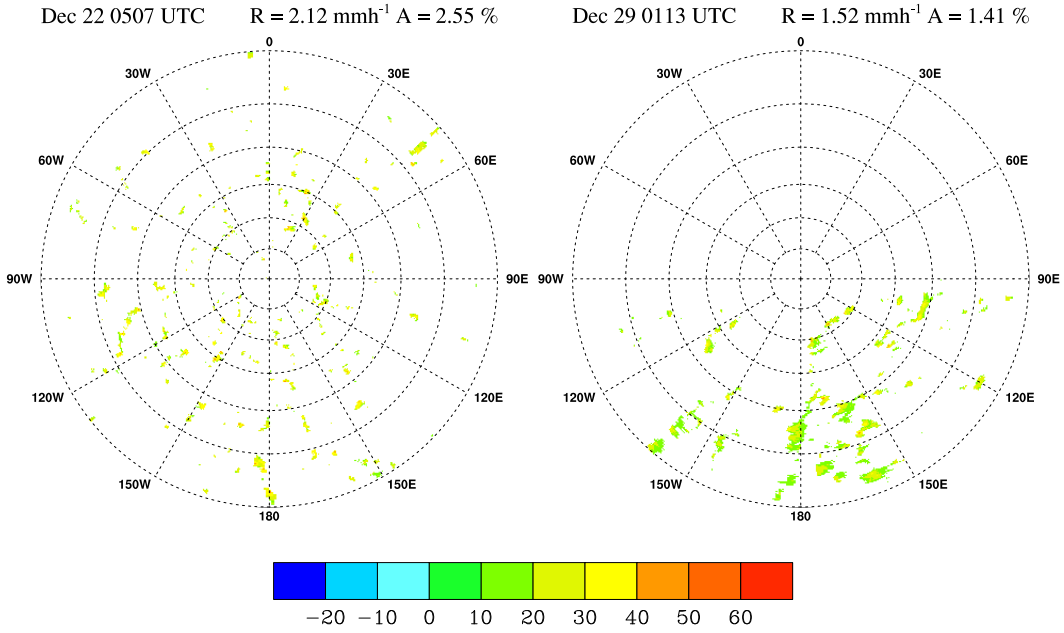

Figure 4.6: Radar surveillance scan of 2004/12/22 (05:07 UTC) and 2004/12/29 (01:13 UTC). Given at the top right are the average R_{echo} (here as R) and the echo coverage (here as A).

All the days that are still included are labeled as 'shallow cumulus' days for now. Based on the histogram anomalies that revealed how days may differ with regard to their actual rain rates (R_{echo}), a distinction can be made between the excluded days (seven in total). At first, days with a high R_{echo} are characerized by deeper cumulus of even cumulonimbus clouds. These days are the 13^{th}, 14^{th}, 15^{th} of December and the 13^{th}, 14^{th}, 18^{th} of January. Satellite images and flight and weather reports are also used for verification. Keep in mind that by referring to these clouds as deep clouds, it is not meant that they can be compared to the deep convective clouds in the ITCZ regions. Yet only one day remains, namely January 9^{th}, when the R_{echo} is actually quite low, but the coverage is extremely high. This day, with an extensive stratocumulus-like cloud deck, is therefore treated separately. However, because it is just one day, it is probably less reliable.

Yet a general distiction is made into three types, for which daily rain rates and echo coverage are averaged and given in Table 4.3. The average echo coverage of 0.71 % and echo rain rate of 1.238 mm h^{-1} for shallow clouds are especially interesting to point out. If one considers cloud fractions near 10 % to be typical for shallow cumulus, the average coverage indicates that roughly one tenth of a cloud is precipitating. Furthermore, the average rain rate of 1.238 mm h^{-1} can be expected to have a significant influence on the development of a cloud, considering that 1 mm h^{-1} corresponds to about 750 Wm^{-2} in energetic terms. Specifically, the development of cloud by itself can influence the development of the boundary layer and thereby also indirectly the surface evaporation and the hydrological cycle.

These values clearly show how the shape of a reflectivity histogram, in combination with the echo coverage, influences the rain rates. Perhaps in a following more comprehensive

analysis, different cloud types need be taken into account, by for example applying different Z - R relations. However, it is remarkable that although the R_{area} for the deeper cumulus is considerably larger than R_{area} for the shallow cumulus, their R_{echo} does not differ that significantly. One may wonder whether the cloud structure really differs during those days. Perhaps it can even be concluded that the (vertical) cloud structure does not influence the rain rates that much at all for shallow clouds.

Of course these values are just based on daily averages. If the radar data is analyzed scan-by-scan, more information about the relation between cloud types and the corresponding rain rates may be obtained. The echoes on a radar scan may not reveal all the information about cloud structure, but it can be very interesting to study them in more detail. For example, do the echoes appear as small echo cells, smaller than a couple of kilometers in diameter? Are they scattered over the radar domain or rather concentrated in a line of echoes? Or is a radar image characterized by a large rain band of tens of kilometers in diameter?

Cloud type	**Echo coverage** [%]	**Area rain rate** [mm h^{-1}]	**Echo rain rate** [mm h^{-1}]
shallow cumulus	0.71	0.011	1.238
deep cumulus - cumulonimbus [1]	7.43	0.135	1.850
stratocumulus - cumulus [2]	23.82	0.241	1.082

1) 13th, 14th, 15th of December and 13th, 14th, 18th of January
2) 9th of January

Table 4.3: The average echo coverage and rain rates are given for three general cloud types observed during the field campaign.

In Figure 4.6 two radar scans of filtered data are shown, for December 22nd (05:07 UTC) and 29th (01:13 UTC). The coverage (here given as A) and the average R_{echo} of the echoes on these particular scans are given above each figure. On December 22nd, small echoes that are very equally distributed, and perhaps even difficult to distinguish, dominate the radar domain. Although each of them is small, their total coverage is 2.55 % and the intensity of rain produced in the clouds even reaches an average of 2.12 mm h^{-1} . On the scan of December 29th, larger echoes or maybe rain bands are present, only dominating the south of the radar domain. Both the coverage and the R_{echo} are smaller, being 1.41 % and 1.52 mm h^{-1} respectively.

Consequently, even when the sky is dominated by fair weather trade-wind cumulus clouds and echoes are so small you can hardly observe them on a scan, the total amount of rainfall may not be negligible, as shown by these examples.

Chapter 5

Summary and recommendations

The prevailing easterly flow in the trade-wind regions induces convection from the ocean's surface, resulting in extensive fields of shallow cumulus clouds. These clouds are effective evaporators and moisten the boundary layer in the trade-wind region. Thereby they fuel the deep convection in the tropics and are important for the global Hadley circulation. Recently, the role of shallow clouds is put in a larger scale perspective and the influence of these clouds on the hydrological cycle and global circulations on earth is questioned. In addition, the significance of precipitation from shallow clouds has received more attention. In December 2004 and January 2005 the Rain In Cumulus over the Ocean (RICO) field study was conducted to study shallow cumulus clouds and associated precipitation processes. RICO took place in the trade-wind region in the vicinity of the Eastern Caribbean islands Antigua and Barbuda. Instrumentation that was implemented to measure precipitation during RICO included the ground-based S-PolKa radar and rain gauges at a surface station and the research ship.

The research described in this report is directed toward giving first estimates of precipitation from shallow cumulus clouds in the trade wind region. The S-PolKa radar observations of rainfall have been used, while this radar offers rainfall statistics with both a high resolution in time and space and a high coverage. The S-PolKa radar scanned an area up to 150 km in radius, for a time period of slightly more than two months. Only the horizontal radar scans have been analyzed, as these scans allow to observe rainfall below cloud base even at large distances from the radar. This analysis has given promising results about the significance of rainfall in a region that has not been studied before on this scale and with this objective.

The time series of rainfall during RICO shows that precipitation from shallow clouds is prevalent. The small rain peaks can certainly not be considered negligible, as for instance all the peaks in area rainfall below 0.125 mm h^{-1} contribute up to 50% of the total rainfall in the whole area. The rainfall observed by the radar coincides to a high extent with the rain gauge measurements at the surface station, indicating that precipitation occurs with such considerable rain rates that it does not completely evaporate before reaching the surface. The radar derived rain rates may therefore be a good impression of the local surface precipitation.

The observed rainfall has an average area coverage of 0.71 %. If a typical cloud fraction is about 10 %, this indicates that precipitation is an order of magnitude less common than clouds. The average actual rain rate in a typical shallow cloud is found to be 1.238

mm h^{-1} . The rain rates produced by these shallow clouds may be relatively small compared to the heavy rain produced by deep convective clouds, but they can be categorized as heavy drizzle or very light rain. Rain rates of 1.238 mm h^{-1} can have a significant effect on the development of the cloud and hence the boundary layer and indirectly the surface evaporation.

This data analysis has provided new insights and has lead to new issues that can be explored in future studies. A list of recommendations follows below:

1. The filtering of Bragg scattering can be improved. With the use of the current threshold value of 10 db$Z$ possible Rayleigh scattering is filtered as well. By fitting a log-normal distribution to the unfiltered reflectivities above 0 db$Z$ in the histogram of Figure 3.3(b) (in paragraph 3.1.3.2), the contributions of Rayleigh and Bragg scattering in the distributions below 0 db$Z$ can be more accurately separated.

2. With the use of a single Z - R relation, it is assumed that drop size distributions do not differ in time and space, which is of course not the case. Using different Z - R relations for different cloud types and heights in the atmosphere would improve the estimation of rain rates. As the center of the radar beam is located at higher altitudes with increasing range, the Z - R relation is expected to change (especially when scans are made with a high elevation angle). The analysis of rainfall observations and drop size distributions in clouds, as measured by instruments on board of the aircrafts, can lead to the development of specific Z - R relations for precipitation in trade-wind cumulus. With such relations a more accurate estimation of rainfall with S-PolKa radar data can be obtained.

3. The relation between echo coverage and area and echo rain rates can be compared more critically, for example by evaluating correlations. This can provide better insight in the influence that the organization of rain echoes and localized heavy rainfall may have on the total area rainfall.

4. It is worthwhile to study how significant the differences are between rainfall in the areas upwind and downwind of Barbuda, as shown in paragraph 4.2.4. For the RICO student research, aimed at understanding the processes controlling the development of the tail clouds downwind of the Caribbean islands, the radar data can provide detailed information of the precipitation associated with these tail clouds.

5. In this study it is assumed that the small rainfall peaks are related to shallow cumulus clouds. However, this is not verified with information about cloud depth or the height of the inversion. This can be done by relating the available sounding data to this dataset. One could also think of relating rainfall statistics to cloud diameter and cloud fraction. Combining all this type of information in one dataset can be particularly useful for comparison with modeling studies of shallow cumulus and associated precipitation processes (for example LES studies).

6. It will be very interesting to formulate a characterization of the organization and shape of the rain echoes on radar images and relate this to the estimated rain rates. By doing so, perhaps one could get more insight in the ways precipitation may affect

cloud structure. Furthermore, if the structure of rain echoes is a good indication of the structure of clouds, a characterization could help to understand how the organization of clouds and regions of rain are influenced by the large-scale synoptic situation.

7. When extending the study to the use of vertical radar scans, it is useful to include the K-Band radar data. From this data information can be obtained about cloud structure. In addition, in combination with S-Band, K-Band can be used to detect Bragg scattering.

8. It is interesting to further explore how the shallow precipitation estimates from the S-Pol radar and space-borne remote sensing techniques, such as GPCP satellite analysis and the TRMM precipitation radar, compare. The S-Pol rainfall estimates can for instance be compared with climatological data from the TRMM precipitation radar, for the specific area observed by S-Pol.

9. The amount of precipitation from shallow cumulus that actually reaches the surface can be quantified further, for instance by analyzing the radar observations of rainfall in the vertical radar scans. It will make a difference to the energy budget whether precipitation evaporates below cloud base or whether it reaches the ocean's surface. In both ways, the depletion of moisture will affect the development of clouds and the deepening of the boundary layer, and hence indirectly the surface evaporation. However, with the evaporation of precipitation above the surface, the generation of cold pools can start to play an important role as they trigger the development of new clouds.

10. To test the hypothesis that an increase of sea salt particles at times of high wind speeds results in bigger cloud droplets and more rainfall, one can relate the radar derived rain rates to measurements of aerosol concentrations.

Acknowledgments I wish to thank Bjorn Stevens for advising me during my stay at the University of California (UCLA) and for giving me the opportunities to explore my research. His endless enthusiasm and ideas have been and are still a great encouragement. My appreciation goes to both Bjorn Stevens and Jordi Vilà, who have given me the opportunity to participate as a student in the RICO field study. Due to the RICO Graduate Seminar Series and student research flight, that were made possible by many of the researchers involved in the field phase of RICO, I have experienced research in a very unique way. I would also like to thank Jordi Vilà for his helpful comments and ongoing interest in my research, even if it was just by email contact.
All the graduate students at UCLA are thanked for the good times beside work, and especially Brian Medeiros for his comments on my research and for all the practical help during both RICO and my time at UCLA. Remco Uijlenhoet has provided useful information about Z - R relations during this research. Finally, proofreading by Peter Nuijens and Dirk Steenbergen provided many comments that have led to an improvement of this report. This research has been supported by the National Science Foundation through grant ATM-0342625.

Appendix A

Radar reflectivity If targets in a unit volume of air scanned by the radar have a diameter D less than a tenth of the radar's wavelength, Rayleigh theory can be applied to the scattering caused by these targets. With this theory, a target is assumed to scatter the radar signal equally in all directions , *i.e.* isotropic scattering. σ is the cross-sectional area that an isotropic scatterer needs to produce the same scattering by the actual target that may scatter anisotropic. It is given by the following equation:

$$\sigma = \frac{\pi^5 |K|^2 D^6}{\lambda^4} \tag{5.1}$$

where $|K|^2$ is a function of the complex index of refraction of the scatterer's substance (the dielectric factor) and λ is the wavelength of the radar.

The reflectivity η_r is then defined as the sum of all the backscattering cross sections $\sum \sigma$ of the individual scatterers within the radar volume:

$$\eta = \frac{\pi^5 |K|^2}{\lambda^4} \sum D^6 \tag{5.2}$$

$\sum D^6$ refers to the sum of the sixth powers of the diameters of all the targets in the radar volume.

The average returned power $\overline{P}_r$ of the radar, at a certain range r at which the resolution volume V_{res} is centered, depends on both the reflectivity η_r from targets in that volume and on the radar equipment; for example the radar wavelength, the transmitted power, the beam width and antenna gain. The returned power by the radar is usually expressed as the more familiar *radar reflectivity factor* Z with units of $\mathrm{mm}^6\,\mathrm{m}^{-3}$:

$$Z \equiv \frac{1}{V_{res}} \sum D^6 = \frac{r^2 \overline{P}_r C_R}{|K|^2} \tag{5.3}$$

where C_R is a constant depending on the radar equipment.

The value of $|K|^2$ is often chosen to be 0.93, the value for liquid water, since normally the exact composition of the scatterers is not known. Reflectivity is therefore sometimes expressed as the equivalent reflectivity Z_e, the value returned when the scatterers would consist purely of liquid water. (Rogers and Yau 1989; Houze 1993; Knight and Miller 1993).

Radial velocity Both clear air echoes and precipitation echoes in a radar scan can be used to obtain information about the motion of the air in which they are located. This is

done by using the shift in the Doppler frequency. Because the radar scans used are nearly horizontal, the motion of targets along the radar beam represents the ambient wind and consequently the horizontal wind field (speed and direction) can be estimated. If a target is moving, the phase ϕ_p of the reflected signal will change with time. This Doppler phase shift is given by:

$$\frac{d\phi_p}{dt} = \frac{4\pi V_R}{\lambda} \tag{5.4}$$

from which the radial velocity V_R in $\mathrm{m\,s^{-1}}$ can be derived. The radial velocity that is returned as a variable by the radar is actually an estimate of the mean radial velocity, since targets may be moving with different velocities.

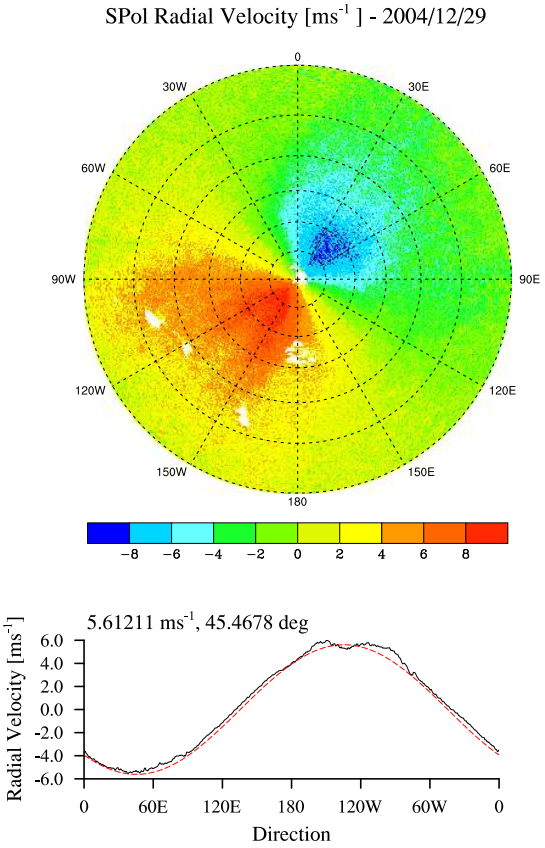

Figure 5.1: The top plot shows a radar surveillance scan of the daily average radial velocity field for 2004/12/29. The bottom plot represents the sine wave (in black) of this radial velocity field along a circle. In red the best fitting sinusoid is given. The calculated wind speed and direction are 5.6 $\mathrm{m\,s^{-1}}$ and 45.5 deg.

On a radar image, targets moving towards the radar have a negative radial velocity, while targets moving away from the radar have a positive velocity. The radial velocity along a concentric circle of a wind field, appearing on a 360° radar surveillance scan, can thus be described by a sine wave. To realize this, the radial velocity at every angle is averaged

over range and Fourier analysis is applied to get the best fitting sinusoid. In Figure 5.1 both the daily average radial velocity field of a radar scan of December the 29th and the fitting sinusoid for that scan are shown. The amplitude of this sinusoid then corresponds to the wind speed and the phase of the sinusoid to the wind direction (Houze 1993).

The Z - R relation The radar reflectivity Z in 5.3 can also be expressed as an integral:

$$Z = \int_0^\infty D^6 N(D) dD \tag{5.5}$$

where $N(D)dD$ is the number of particles per unit volume with diameters ranging from D to $D + dD$, *i.e.* the particle size distribution. For raindrops, $N(D)dD$ is the rain drop size distribution.

The rain rate R is defined as follows:

$$R = \frac{\pi \rho_L}{6} \int_0^\infty V(D) D^3 N(D) dD \tag{5.6}$$

where $V(D)$ is the fall velocity that is related either empirically or theoretically to the diameter D. ρ_L is the density of liquid water.

Because both Z and R are related to the diameter D an empirical relation between the two exists:

$$Z = \alpha R^\beta \tag{5.7}$$

In-situ measurements of the drop size distribution can be used to estimate the coefficients α and β (Rogers and Yau 1989; Houze 1993).

Bibliography

Battan, L., 1973: *Radar observations of the atmosphere*. p. 324 pp. University of Chicago Press.

Caesar, K., 2005: Summary of the weather during the RICO project.

Houze, R., 1993: *Cloud dynamics*. chapter 4: Radar meteorology. Academic Press, 1st edition.

Jensen, J., S. Lee, P. Krummel, J. Katzfey and D. Gogoasa, 2000: Precipitation in marine cumulus and stratocumulus. part I: Thermodynamic and dynamic observations of closed cell circulations and cumulus bands. *Atmospheric Research*, **54**, 117–155.

Johnson, R., P. Ciesielski and J. Cotturone, 2001: Multiscale variability of the atmospheric mixed layer over the western Pacific warm pool. *J.Atmos.Sci.*, **58**, 2729–2750.

Johnson, R. and X. Lin, 1997: Episodic trade wind regimes over the western Pacific warm pool. *J.Atmos.Sci.*, **54**, 2020–2034.

Knight, C. and L. Miller, 1993: First radar echoes from cumulus clouds. *J.Atmos.Sci.*, **74**(2), 179–188.

Knight, C. and L. Miller, 1998: Early radar echoes from small, warm cumulus: Bragg and hydrometeor scattering. *J.Atmos.Sci.*, **55**, 2974–2992.

Lau, K. and H. Wu, 2003: Warm rain processes over tropical oceans and climate implications. *Geophys.Res.Lett.*, **30**(24).

LeMone, M. and W. Pennell, 1976: The relationship of trade wind cumulus distribution to subcloud layer fluxes and structure. *Mon.Wea.Rev.*, **104**, 524–539.

Neggers, R., 2002: *Shallow cumulus convection*. Ph.D. thesis, Wageningen University.

Petty, G., 1999: Prevalence of precipitation from warm-topped cumulus clouds over eastern Asia and the western Pacific. *J.Climate*, **12**, 220–229.

Rauber, R., C. Knight, H. Ochs and B. Stevens, 2004: Rain In Cumulus over the Ocean experiment. Scientific overview submitted to NSF.

Rickenbach, T. and S. Rutledge, 1998: Convection in TOGA COARE: Horizontal scale, morphology, and rainfall production. *J.Atmos.Sci.*, **55**, 2715–2729.

Rogers, R. and M. Yau, 1989: *A short course in cloud microphysics*. chapter 11: Weather radar. Butterworth-Heinemann, 3rd edition.

Rosenfeld, D. and C. Ulbrich, 2003: Cloud microphysical properties, processes, and rainfall estimation opportunities. *Meteorological Monographs*, **52**, 237–258.

Schumacher, C. and R. Houze, Jr., 2003a: Stratiform rain in the tropics as seen by the TRMM precipitation radar. *J.Climate*, **16**, 1739–1756.

Schumacher, C. and R. Houze, Jr., 2003b: The TRMM precipitation radar's view of shallow, isolated rain. *J.Appl.Meteor.*, **42**, 1519–1524.

Short, D. and K. Nakamura, 2000: TRMM radar observations of shallow precipitation over the tropical oceans. *J.Climate*, **13**, 4107–4124.

Siebesma, A. et al., 2003: A large eddy simulation intercomparison study of shallow cumulus convection. *J.Atmos.Sci.*, **60**, 1201–1219.

Steiner, M., J. Smith and R. Uijlenhoet, 2004: A microphysical interpretation of radar reflectivity - rain rate relationships. *J.Atmos.Sci.*, **61**, 1114–1131.

Stevens, B., 2005: Atmospheric moist convection. In press for *Annu.Earth Planet.Sci.*

Tokay, A. and D. Short, 1996: Evidence from tropical raindrop spectra of the origin of rain from stratiform versus convective clouds. *J.Appl.Meteor.*, **35**, 355–371.

Tompkins, A., 2001: Organization of tropical convection in low vertical wind shears: the role of cold pools. *J.Atmos.Sci.*, **58**, 1650–1772.

TRMM PR Instruction Manual, 2004: *Tropical Rainfall Measuring Mission (TRMM) Precipitation Radar Algorithm - Instruction Manual*. Japan Aerspace Exploration Agency (JAXA) and National Aeronautics and Space Administration (NASA), Manual Version 1.

Uijlenhoet, R., 2004: Parameterization of raindrop size distributions and radar reflectivity - rain rate relationships. Contribution to ERAD 2004 Introductory course to radar precipitation estimation.

Van Zanten, M., B. Stevens, G. Vali and D. Lenschow, 2005: Observations of drizzle in nocturnal marine stratocumulus. *J.Atmos.Sci.*, **62**, 88–106.

Wu, Z., 2003: A shallow CISK, deep equilibrium mechanism for the interaction between large-scale convection and large-scale circulations in the tropics. *J.Atmos.Sci.*, **60**, 377–392.